J Mater Sci (2007) 42:6453–6463
DOI 10.1007/s10853-006-0673-8

Investigation of solid solution of ZrP_2O_7–$Sr_2P_2O_7$

Semih Seyyidoğlu · Macit Özenbaş · Necmeddin Yazıcı · Ayşen Yılmaz

Received: 1 March 2006 / Accepted: 14 July 2006 / Published online: 14 April 2007

Abstract In this study, ZrP_2O_7 was synthesized by the solid state reaction of ZrO_2 and $NH_4H_2PO_4$ at 900 °C. Then, in set 1; 10, 5, 1, 0.5, 0.1, 0.05, 0.03% previously prepared $Sr_2P_2O_7$ were doped into ZrP_2O_7, and $Sr_2P_2O_7$ slightly affect the unit cell parameter of cubic ZrP_2O_7 (a = 8.248(6)–8.233(8) Å). The reverse of this process was also applied to $Sr_2P_2O_7$ system (set 2). ZrP_2O_7 changes the unit cell parameters of orthorhombic $Sr_2P_2O_7$ in between a = 8.909(5)–8.877(5) Å, b = 13.163 (3)–13.12(1) Å, and c = 5.403(2)–5.386(4) Å. Analysis of the vibrations of the $P_2O_7^{4-}$ ion and approximate band assignments for IR and Raman spectra are also reported in this work. Some coincidences in infrared and Raman spectra both sets were found and strong P–O–P bands were observed. Surface morphology, EDX analysis, and thermoluminescence properties of both sets were given the first time in this paper.

Introduction

Pyrophosphates are technologically important materials due to their applications as ceramic, catalysts, ion exchange and optical materials. Because of their potential applications, many researchers synthesized either single crystal or powder pyrophosphates. These pyrophosphates generally were found in literature containing different formula group. Among these, one is $M^{IV}P_2O_7$ (M^{IV} is tetravalent), and the other is $M^{II}{}_2P_2O_7$ (M^{II} is divalent), and $M^{I}M^{III}P_2O_7$ (mixed valance). The cubic ZrP_2O_7 is one of the most known pyrophosphate in $M^{IV}P_2O_7$ type. Symmetry characterization of cubic ZrP_2O_7 was studied by Withers et al. [1] and Sleight and co-workers [2] investigated unusual P–O–P bond angles in cubic ZrP_2O_7. The crystal structure of novel cubic pyrophosphate WP_2O_7 [3] was reported by Lisnyak's group. Phase transition studies of pseudocubic SnP_2O_7 was published by Gover et al. [4].

In the second formula group, the $[P_2O_7]^{4-}$ group containing divalent metals are given. Triclinic tin (II) pyrophosphate $Sn_2P_2O_7$ single crystals were obtained in argon flow in Shapanchenko's group [5]. Another divalent metal containing triclinic pyrophosphate was obtained by Guler and Kurtulus [6]. He followed microwave-assisted route to synthesize $Pb_2P_2O_7$. Besides these divalent metal containing pyrophosphates, Smaalen's group synthesized orthorhombic vanadyl pyrophosphate $(VO)_2P_2O_7$ by heating $VO(PO_4)\cdot 0.5H_2O$ under argon atmosphere [7].

The mixed valance metal containing group is the largest member of pyrophosphates. Kizilyalli and co-workers synthesized orthorhombic $NaGdP_2O_7$ by using solid state [8] and orthorhombic $HGdP_2O_7$ [9] by precipitation methods. Similarly, tetragonal $NaDyP_2O_7$ [10], orthorhombic $NaLaP_2O_7$ [11], monoclinic $NaEuP_2O_7$ [12], and orthorhombic KYP_2O_7 [13] were obtained by many researchers. Single crystals of

S. Seyyidoğlu · A. Yılmaz (✉)
Department of Chemistry, Middle East Technical University, 06531 Ankara, Turkey
e-mail: ayseny@metu.edu.tr

M. Özenbaş
Department of Metallurgical and Materials Engineering, Middle East Technical University, 06531 Ankara, Turkey

N. Yazıcı
Department of Engineering Physics, Faculty of Engineering, Gaziantep University, Turkey Gaziantep 27310, Turkey

$K_2SrP_2O_7$ [14], $Rb_2SrP_2O_7$ and $CsSrP_2O_7$ [15] were synthesized by Trunov. Another crystal work was done by Raveau and coworkers. They synthesized monoclinic $LiMoP_2O_7$ [16] single-crystals by controlled cooling. Same procedure was applied by Holt and triclinic $PbFe_2(P_2O_7)_2$, monoclinic $BaFe_2(P_2O_7)_2$ [17], and monoclinic $CuFe_2(P_2O_7)_2$ [18] were produced. Another kind of diphosphate materials with the general formula $RbLnP_2O_7$ (where Ln = Dy, Ho, Y Er, Tm, Yb) [19], $CsLnP_2O_7$ (where Ln = Gd, Tb, Dy, Ho, Y Er, Tm, Yb) [20], and α-$Ca_2P_2O_7$, $CaCuP_2O_7$, $SrCuP_2O_7$, $SrCdP_2O_7$, $BaMgP_2O_7$ [21] have been deal of many studies. Hydrothermal synthesis of monoclinic $Na_2CrP_2O_7{\cdot}0.5H_2O$ was achieved by Stock et al. [22]. A new, dicationic, and acidic orthorhombic $KHMgP_2O_7$ was obtained by Butler and his co-workers [23]. A series of compounds $(M^a_{0.5}M^b_{0.5})P_2O_7$, M^aM^b = AlTa, FeTa, GaTa, InNb, YNb, NdTa, and BiTa that are close structural relatives of cubic ZrP_2O_7 were prepared by Varga et al. [24].

Among these pyrophosphates there were very few publications in literature about the properties of zirconium and strontium pyrophosphates. Emission spectra of ZrP_2O_7 activated with Eu^{3+} and Tb^{3+} was investigated by Pelova and Grigorov [25] and dielectric properties of ZrP_2O_7 was investigated by Kim and Yim [26]. Besides these, zirconium pyrophosphates are used as catalyst in *n*-butane oxidative dehydration [27] and used as a new packing material for high performance liquid chromatography [28]. Prasad and co-workers investigated preparation and ammoxidation functionality of zirconium phosphate-supported V_2O_5 catalysts [29]. They reported that the V_2O_5/ZrP_2O_7 catalysts are found to be highly active and selective. Also, crystal structure and phase transitions of strontium zirconium diorthophosphate, $SrZr(PO_4)_2$, was published recently [30] while europium-ion doped strontium pyrophosphate and its photoluminescence work was done by Lu's group [31].

However, no attempt of ZrP_2O_7–$Sr_2P_2O_7$ solid solution of has yet been reported. In the present study, we established two sets of products by doping $Sr_2P_2O_7$ into ZrP_2O_7 with 10, 5, 1, 0.5, 0.1, 0.05, 0.03% and reverse of this process was applied to $Sr_2P_2O_7$ to describe the unit cell, vibrational, morphological, and thermoluminescence changes in these two sets.

Experimental

The ZrO_2, $SrCO_3$, and $NH_4H_2PO_4$ (from Merck, Aldrich and Allied Chem.) solid powders were used in the solid state reactions. All preparations were made by spontaneous crystallization in oxygen atmosphere. Stoichiometric amounts of reactants and heat treatment details are given in Table 1. Desired quantities of initial reactants were weighed separately and crushed well in agate mortar. Then the mixture was transferred into a porcelain crucible and put into a furnace for heating. The solid state reactions have been carried out in air with the aid of muffle furnaces. The products were subjected to X-ray powder diffraction and IR analysis after each sintering process.

Table 1 Name, composition, and heating treatment of (a) set 1 and (b) set 2

Exp. No	Composition	900 °C
(a) Set 1		
D30	ZrP_2O_7	14.5 h
D32	ZrP_2O_7:10% $Sr_2P_2O_7$	10.5 h
D33	ZrP_2O_7:5% $Sr_2P_2O_7$	10.5 h
D34	ZrP_2O_7:1% $Sr_2P_2O_7$	10.5 h
D35	ZrP_2O_7:0.5% $Sr_2P_2O_7$	10.5 h
D36	ZrP_2O_7:0.1% $Sr_2P_2O_7$	10.5 h
D37	ZrP_2O_7:0.05% $Sr_2P_2O_7$	10.5 h
D38	ZrP_2O_7:0.03% $Sr_2P_2O_7$	10.5 h
(b) Set 2		
D31	$Sr_2P_2O_7$	14.5 h
D39	$Sr_2P_2O_7$:10% ZrP_2O_7	10.5 h
D40	$Sr_2P_2O_7$:5% ZrP_2O_7	10.5 h
D41	$Sr_2P_2O_7$:1% ZrP_2O_7	10.5 h
D42	$Sr_2P_2O_7$:0.5% ZrP_2O_7	10.5 h
D43	$Sr_2P_2O_7$:0.25% ZrP_2O_7	10.5 h
D44	$Sr_2P_2O_7$:0.1% ZrP_2O_7	10.5 h
D45	$Sr_2P_2O_7$:0.05% ZrP_2O_7	10.5 h

X-ray Powder patterns (XRD) were taken by using Rigaku Miniflex Diffractometer with and Cu K_α (30 kV, 10 mA, $\lambda = 1.54051$ Å) radiation. Scanning was generally done between $5° < 2\theta < 70°$. The precise peak positions were determined by means of the fitting program CELREF [32], yielding the least squares refinement of the lattice parameters. Nicolet 510 FTIR Infrared Spectrometer was used in the region 400–1,500 cm^{-1}. Spectroscopic grade KBr was used for making IR pellets. It was dried at 180 °C for about 1 day before using. The ratio of KBr to sample was 100 mg:3 mg. In Raman analysis, Jobin Yvon-Horiba with Andor CCD was used in the region 50–1,200 cm^{-1}. Scanning Electron Micrographs were taken by JEOL JSM 6400 (20 kV), equipped with NORAN system 6 X-ray Microanalysis System and Semafore Digitizer. The microscope is equipped with secondary and backscattered electron detectors and X-ray microanalysis system, and is capable of providing both topographical and compositional information about the specimen. Samples were coated with a very thin layer of gold by using HUMMLE VII Sputter Coating Device (ANATECH).

In thermoluminescence (TL) analysis, the prepared samples were irradiated at room temperature with beta rays emitted from a ^{90}Sr–^{90}Y source for 5 min. The time duration between irradiation and TL readout was always kept constant at about 1 min. then the glow curves (GCs) were immediately recorded, so that there was no significant fading of the TL peaks at room temperature. GCs were obtained using a Harshaw QS 3500 manual type reader interfaced to a PC where TL signals were analysed. GC readout was carried out on platinum planchet at linear heating rate 2 °C s^{-1} up to 400 °C.

Results and discussion

X-ray powder diffraction studies

ZrP_2O_7 was synthesized at 900 °C by solid state technique and powder X-ray diffraction studies indicated that the product was essentially a single phase (Fig. 1). The XRD data can be easily indexed into the cubic system with a = 8.248(6) Å (Table 2) and the probable space group is Pa-3. This data is very close to the JCPDS Card No: 24-1491 where a = 8.245 Å. Sleight and co-workers [2] solved the structure of cubic ZrP_2O_7 at room temperature and refined by using a combination of modelling and high-resolution neutron powder diffraction data. The cell edge is 24.74 Å and the space group is Pa-3. They proposed that the $3 \times 3 \times 3$ superstructure present at room temperature disappears at about 290 °C. Withers et al. [1] mentioned that the unmodulated parent structure of zirconium pyrophosphate made up of corner-connected ZrO_6 octahedra and PO_4 tetrahedra projected along an ⟨001⟩ direction. Withers and co-workers also explained that above 294 °C, the parent cell parameter is multiplied by 3 to enable direct comparison with the low-temperature superstructure phase. Therefore, our unit cell and space group data are in agreement with the data of Withers and Sleight.

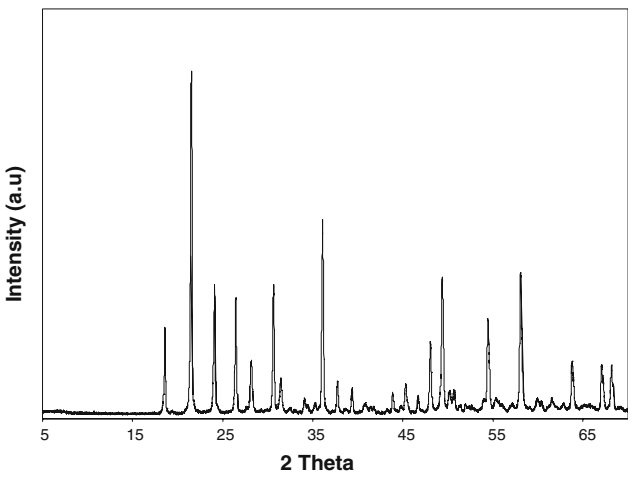

Fig. 1 X-ray powder diffraction pattern of cubic ZrP_2O_7

Table 2 X-ray powder diffraction data of cubic ZrP_2O_7

d_{JCPDS}[24-1491]	d_{obs}	h k l	I/I_0
4.760	4.7612	1 1 1	25
4.13	4.1219	2 0 0	100
3.69	3.6866	2 1 0	38
3.37	3.3644	2 1 1	34
2.915	2.9144	2 2 0	37
2.487	2.4853	2 2 1	57
2.382	2.381	2 2 2	10
2.288	2.2866	2 3 0	7
2.205	2.2072	3 2 1	3
2.062	2.0629	4 0 0	6
2.002	2.0001	4 1 0	9
1.9449	1.9438	1 4 1	5
1.8930	1.8919	3 3 1	21
1.8447	1.8444	2 4 0	38
1.7990	1.8000	2 4 1	6
1.7583	1.7762	3 3 2	2
1.6833	1.6837	2 4 2	27
1.5872	1.5875	1 5 1	40
1.5326	1.5384	2 5 0	3
1.5051	1.5058	2 5 1	4
1.4580	1.4580	4 4 0	15
1.3944	1.3943	3 5 1	13

XRD patterns of set 1 are given in Fig. 2. The unit cell parameters of the set 1 did not change much only in between 8.248(6) and 8.233(8) Å. According to these results it can be said that, in this solid solution, orthorhombic doping did not alter the cubic structure so much. The edge length decreased to 8.233(8) from 8.248(6) Å.

In set 2, $Sr_2P_2O_7$ was synthesized at the same experimental conditions and indexed with respect to JCPDS Card No: 24-1011. The XRD patterns of set 2 were given in Fig. 3. This powder data, which are given in Table 3, were indexed in the orthorhombic system, and the approximate lattice constants were found to be a = 8.900(2), b = 13.151(2), and c = 5.402(2) Å.

In Fig. 4, XRD patterns of set 2 were given. Same trends were observed for three unit cells. They fluctuate in between a = 8.909(5)–8.877(5), b = 13.163(3)–13.12(1), and c = 5.403(2)–5.386(4) Å. Since small fluctuations were observed, it can be concluded that cubic ZrP_2O_7 could not enter the orthorhombic $Sr_2P_2O_7$ structure.

Interpretation of the infrared and Raman spectra

In addition to XRD studies, we measured infrared and Raman spectra of the synthesized products to confirm

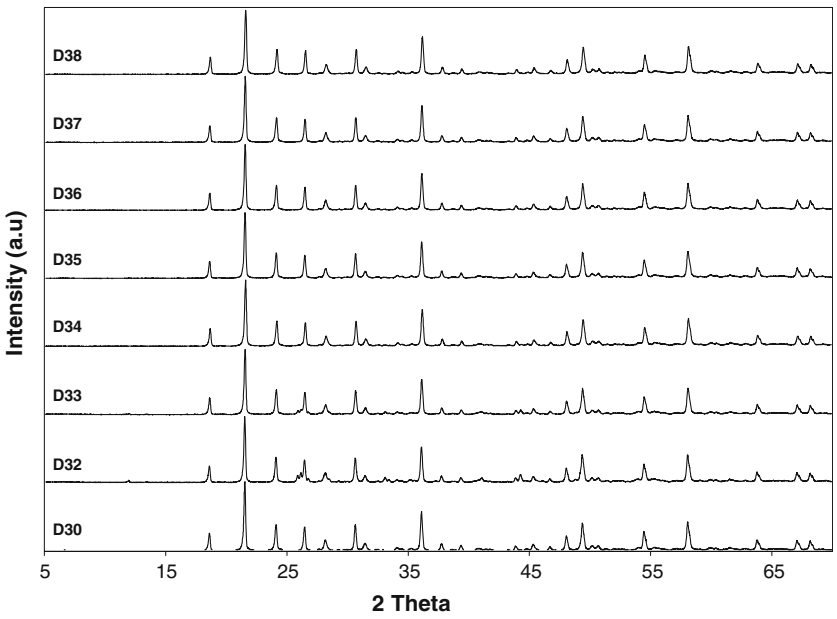

Fig. 2 X-ray powder diffraction patterns of set 1

the functional groups in both sets. The infrared and Raman spectra of the ZrP_2O_7 are shown in Figs. 5, 6, respectively, and Figs. 7, 8 showed the infrared and the Raman spectra of the $Sr_2P_2O_7$. The band positions of the infrared and Raman spectra of the products (set 1 and set 2) obtained in this research are given in Tables 4, 5, respectively. Examination of tables shows that there are some coincidences in the infrared and Raman spectra.

The assignment of the $P_2O_7^{4-}$ modes is carried out in terms of PO_3 and P–O–P vibration [33, 34]. The symmetric and anti-symmetric stretching frequencies of PO_3 in $P_2O_7^{4-}$ are observed in the region 1,157–1,002 cm^{-1}. For POP, symmetric modes were observed in the region 779–736 cm^{-1}. Guler and co-workers [6] observed the bands due to δOPO, δPO_3, δPOP deformations in the region 595–464 cm^{-1}. In our studies, we observed these bands in the between 609 and 455 cm^{-1}.

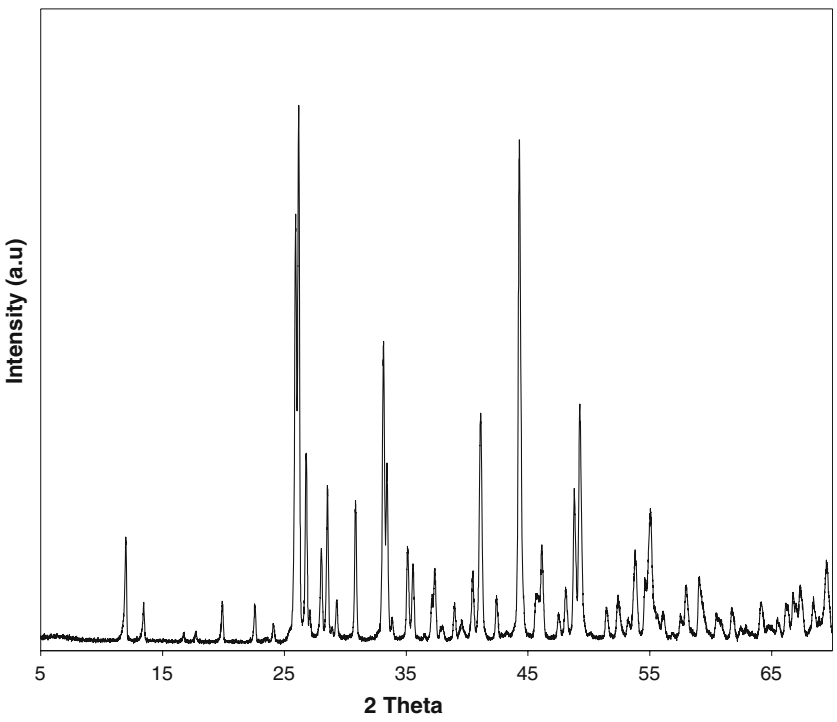

Fig. 3 X-ray powder diffraction pattern of orthorhombic $Sr_2P_2O_7$

Table 3 X-ray powder diffraction data of orthorhombic $Sr_2P_2O_7$

d_{JCPDS}[24-1011]	d_{obs}	h k l	I/I_0	d_{JCPDS}[24-1011]	d_{obs}	h k l	I/I_0
7.4000	7.3750	1 1 0	21	2.2300	2.2270	4 0 0	12
6.6000	6.5727	0 2 0	7	2.1950	2.1933	0 6 0	43
5.3000	5.2790	1 2 0	2	2.1320	2.1295	1 6 0	9
5.0100	4.9898	0 1 1	3	2.0440	2.0434	2 3 2	95
4.4620	4.4511	2 0 0	8	1.9870	1.9856	4 3 0	8
3.9400	3.9327	1 3 0	8	1.9820	1.9807	1 6 1	9
3.6940	3.6911	2 2 0	4	1.9660	1.9665	4 2 1	16
3.4390	3.4345	2 0 1	80	1.9130	1.9129	3 2 2	4
3.4060	3.4010	0 3 1	100	1.8910	1.8908	2 4 2	10
3.3270	3.3237	2 1 1	34	1.8660	1.8649	4 3 1	28
3.2910	3.2864	0 4 0	5	1.8500	1.8489	2 6 1	42
3.1820	3.1806	1 3 1	17	1.7760	1.7759	0 7 1	6
3.1280	3.1249	2 3 0	28	1.7470	1.7458	4 4 1	8
3.0480	3.0445	2 2 1	7	1.7420	1.7434	1 7 1	7
2.9000	2.8959	3 1 0	27	1.7220	1.7211	5 2 0	3
2.7000	2.7009	0 0 2	57	1.7030	1.7031	0 6 2	14
2.6800	2.6789	1 4 1	30	1.6690	1.6695	2 0 3	10
2.6480	2.6474	2 4 0	4	1.6650	1.6667	0 3 3	23
2.5540	2.5537	3 1 1	18	1.6510	1.6524	2 7 1	2
2.5250	2.5231	1 5 0	14	1.6370	1.6380	1 3 3	4
2.4220	2.4206	3 2 1	8	1.6009	1.6011	4 3 2	5
2.4060	2.4055	1 2 2	14	1.5903	1.5900	3 7 0	10
2.3770	2.3773	2 4 1	3	1.5643	1.5635	4 6 0	11
2.3100	2.3086	2 0 2	8	1.5554	1.5582	1 4 3	8
2.2740	2.2767	2 1 2	3	1.5297	1.5301	3 1 3	4
2.2390	2.2365	3 3 1	3	1.5026	1.5014	4 6 1	6

Khay [19, 20] mentioned that the deformation bands are between 630 and 373 cm^{-1} and our peaks around these frequencies are consistent with the literature values. Khay also reported that all bands located below are external vibrational modes. So, the bands below 334 cm^{-1} are external vibrational modes.

Sleight and co-workers [2] observed unusual P–O–P bond angle in ZrP_2O_7. In their work, the $3 \times 3 \times 3$ superstructure present at room temperature disappears at about 290 °C, and all P–O–P angles of P_2O_7 are then constrained by symmetry to be 180 °C on average. In the same study, they also mentioned that the angle for

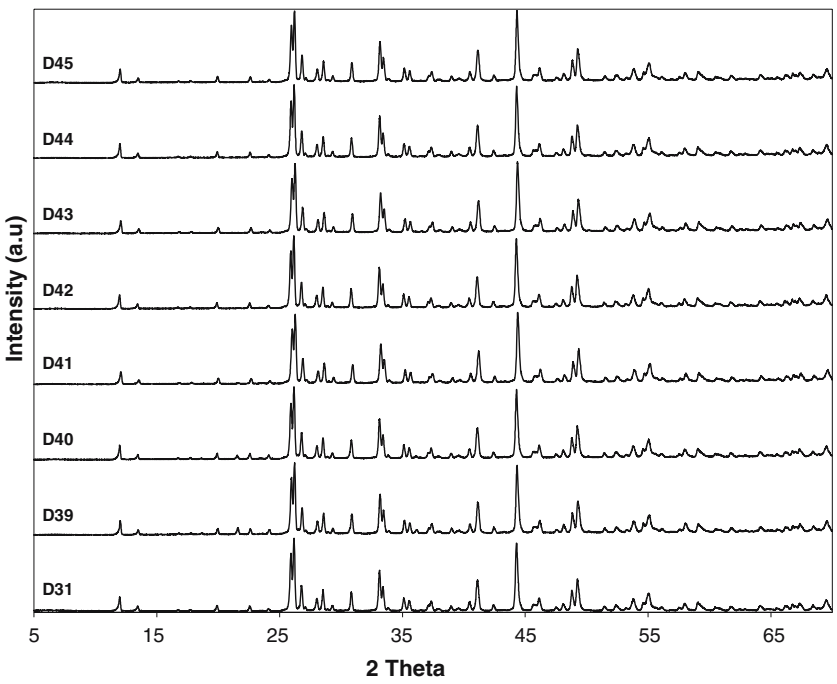

Fig. 4 X-ray powder diffraction patterns of set 2

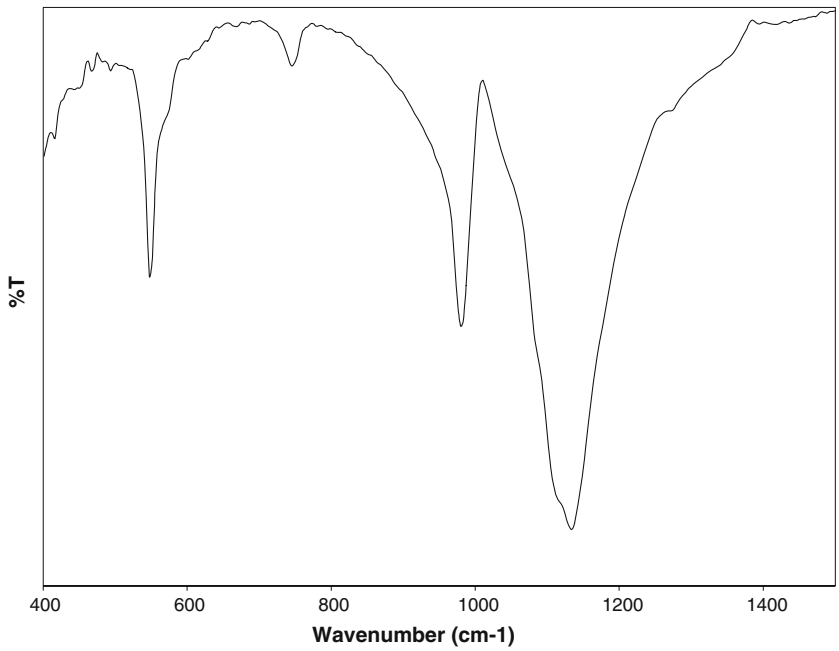

Fig. 5 IR Spectra of cubic ZrP_2O_7

P–O–P linkages is normally in the range 130–160° and the P–O–P bond angle of 180° is unfavourable, and one expects that a structure containing such a linkage could only be stabilized at high temperature. In both sets, our experiments were done at high temperature, we expected to have non-linear POP bond. Baran et al. [34] indicated that for a linear bridge the symmetric mode should be only Raman active and the anti-symmetric mode only IR active. The appearance of both vibrations in both spectra is in an agreement with the presence of an angular bridge. We observed this situation in both the IR and Raman spectra.

The infrared and Raman bands observed are in agreement with the reported values for diphosphate compounds of tetravalent, mixed valent cations [8, 19, 20, 21], although their crystal systems are different.

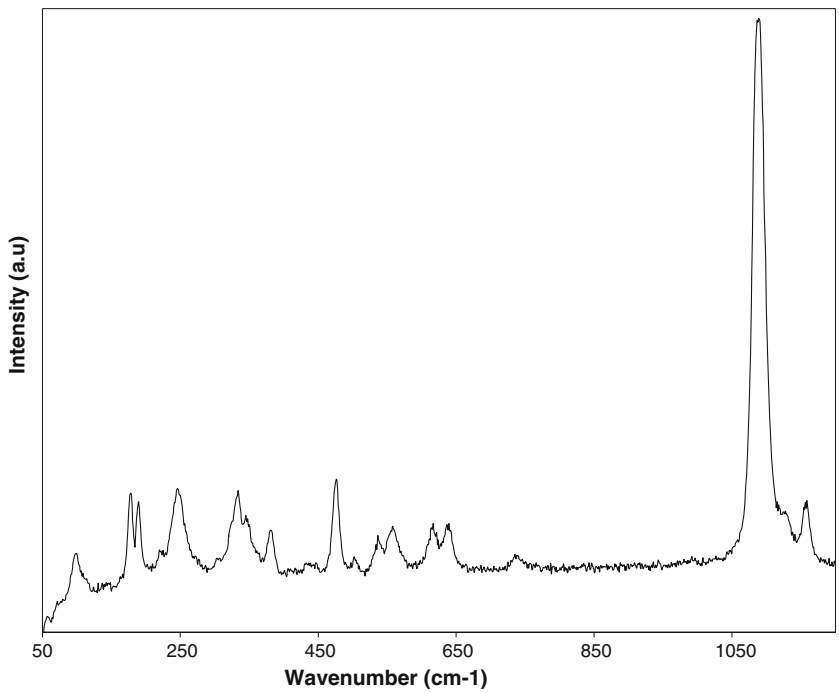

Fig. 6 Raman Spectra of cubic ZrP_2O_7

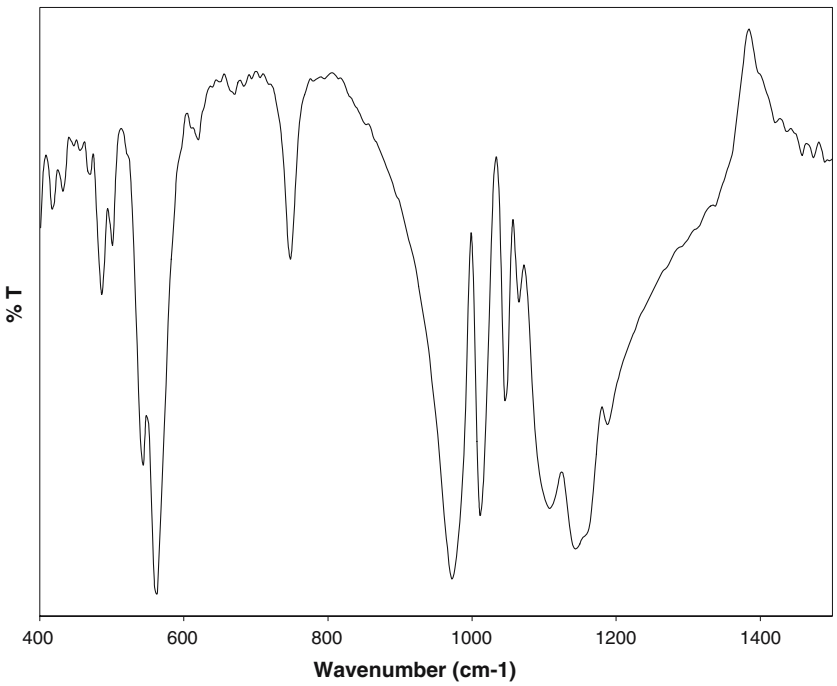

Fig. 7 IR Spectra of orthorhombic $Sr_2P_2O_7$

SEM micrographs and EDX analysis

The morphology of samples set 1 and set 2 were investigated by taking SEM images. The SEM micrographs of pure ZrP_2O_7 and $Sr_2P_2O_7$ were given in Fig. 9. In both figures, SEM images demonstrate the small particle size of these phosphates. In set 1, particles, before and after doping $Sr_2P_2O_7$ to ZrP_2O_7, are around 1 μm. Yet, SEM observations of set 2 showed that one of the remarkable features of these products is that their sizes are larger than set 1.

In Fig. 10, EDX analysis of sample D30, D32 from set 1 and D31, D39 from set 2 are given. In set 1, Sr doping was observed in all samples while the same trend was also investigated in set 2 and Zr doping was seen.

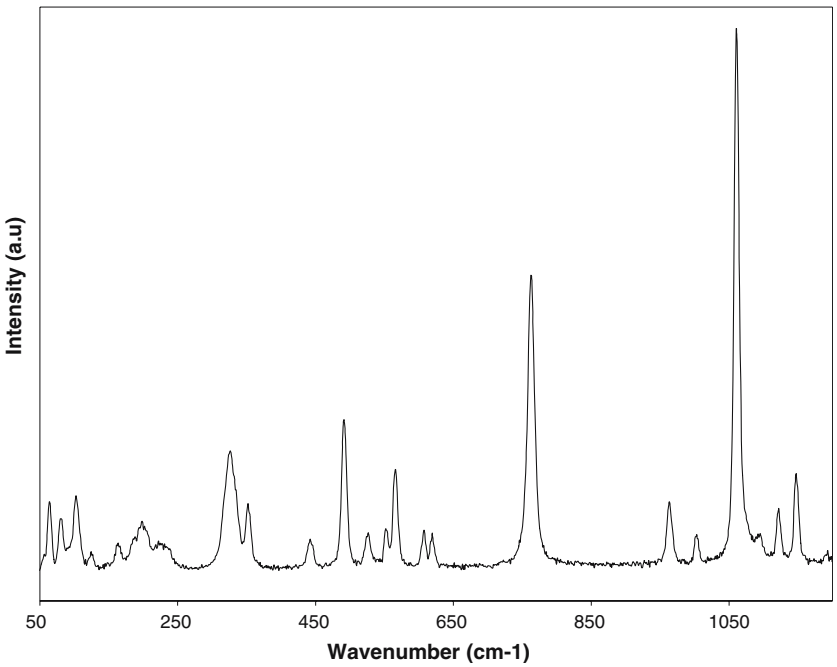

Fig. 8 Raman Spectra of orthorhombic $Sr_2P_2O_7$

Table 4 The band positions for set 1

D30		D32		D33		D34		D35		D36		D37		D38	
IR	R	IR	R	IR	R	IR	R	IR	R	IR	R	IR	R	IR	R
1133	1158	1133	1158	1133	1157	1132	1157	1126	1157	1132	1158	1132	1158	1132	1157
	1088	1115	1090		1086	1115	1089	1112	1089	1115	1089	1115	1089	1113	1087
980		979		980		979		978		979		979		978	
745	735	746	737	746	741	746	736	746	737	746	737	746	742	745	737
643	639		638		638		638		640		638		638		637
600	616		616		614	592	617	595	617		617		615		615
548	557	548	556	548	555	548	556	548	555	548	560	548	556	548	558
	536		537	501	538		537		537	508	538	508	537		535
507	502	500	501		503	502	505		504		503		503		500
493															
483	476	487	476		476		476		476		476		477		475
467				446		446		447		447		447		445	
442				434		437		434		438		438		440	
		433		409		406		409		409		409		409	
415		410													
	380		381		380		382		383		382		382		379
	333		334		333		333		333		333		333		332
	246		249		248		248		248		247		247		245
	189		189		189		191		190		190		190		188
	177		178		177		178		179		179		179		176

Table 5 The band positions for set 2

D31		D39		D40		D41		D42		D43		D44		D45	
IR	R	IR	R	IR	R	IR	R	IR	R	IR	R	IR	R	IR	R
1187	1192	1188	1190	1187	1192	1188	1194	1188	1193	1189	1190	1188	1194	1190	1193
		1155		1155				1156		1157		1156		1157	
1143	1147	1142	1146	1143	1146	1141	1149		1149				1149		1149
1107	1121	1112	1120	1114	1120	1111	1123	1112	1124		1122	1111	1123	1115	1123
	1095		1092		1093		1096		1097				1096		1097
1065		1064		1064		1064		1064		1063		1064		1064	
1046	1060	1046	1060	1046	1060	1046	1063	1046	1063	1046	1060	1046	1063	1046	1062
1011	1003	1011	1002	1011	1002	1011	1004	1011	1004	1011	1003	1011	1004	1011	1004
972	963	970	961	972	962	968	965	969	966	970	963	970	966	970	966
779	762		761		761		765		765		762		764		765
747		747		747		747		747		747		747		747	
683				679											
669		669		669		669		669		669		669		669	
649		652		652		651		651		651		651		651	
619	619	619	617	618	618	619	622	618	622	617	619	619	621	619	621
	607		606		606				609		607		609		609
561	566	560	564	561	565	560	568	560	568	560	565	560	568	560	568
543	551	543	551	543	552	542	555	542	555	543	551	542	555	542	555
	526		526		524		529		528		524		529		528
500	491	501	490	501	490	501	494	500	494	501	491	500	494	500	494
486		485		486		485		485		484		485		485	
469															
456		458		457		456		457		455		458		457	
447	442		443	441	443		446		448		441		446		445
432		433				431		431		434		433		433	
417		419		419		420		420		420		420		419	
	352		351		351		355		355		351		354		355
	326		327		324		328		329		325		328		328
	222		226		225		224		226		222		228		230
	198		202		196		204		201		194		205		200
	163		163		163		166		166		163		166		166
	124		123		125		126		129				127		126

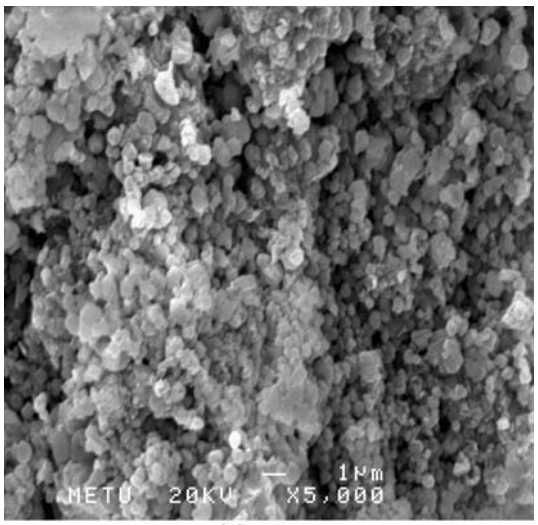

(a) D30

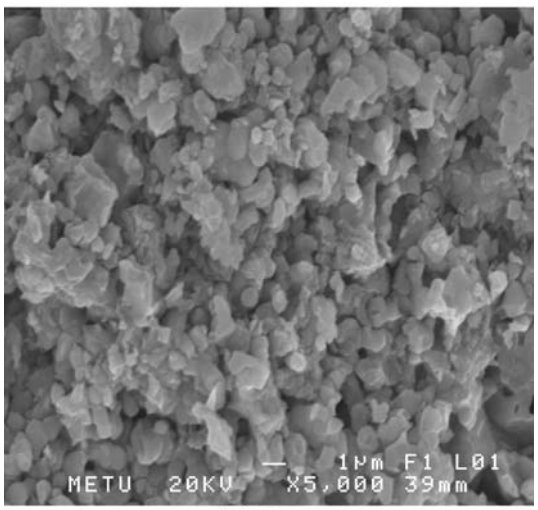

(b) D31

Fig. 9 SEM Micrographs of D30 and D31

Thermoluminescence studies

The TL characteristics of pure and doped strontium pyrophosphate have not been investigated in detail up to now. Lu and his colleagues [30] have recorded the TL glow curve of Eu-doped strontium pyrophosphate and they were reported two glow peaks at 465 and 565 K in the case of samples irradiated by ^{60}Co gamma rays up to 100 and 200 Gy. On the other hand, undoped $Sr_2P_2O_7$ sample did not show any TSL peak. In the present study, all samples were first irradiated for 5 min (≈4.5 Gy) at room temperature in the dark room by β rays and then their glow curves were recorded. As seen in Fig. 11, there is no change in the glow curve structure of all samples in set 2 and their glow curves exhibit one strong glow peak at around 100 °C with low intensity glow peaks at about 200 and 350 °C when the samples heated at a constant heating rate of 2 °C/s. It is seen that the intensity of prominent glow peak at 100 °C is continuously increased with decreasing concentration of ZrP_2O_7 and the maximum TL intensity was observed for the sample D45 (composition $Sr_2P_2O_7$: 0.05% ZrP_2O_7). On the other hand, the peak temperature (T_m) of main peak does not depend on the concentration of ZrP_2O_7 and it becomes constant for all samples in set 2.

Conclusion

In the present study, zirconium pyrophosphate, and strontium pyrophosphate, were synthesized through the following solid state reaction at 900 °C:

$$ZrO_2(s) + 2NH_4H_2PO_4(s) \rightarrow ZrP_2O_7(s) + 3H_2O(g) + 2NH_3(g)$$

$$2SrCO_3(s) + 2NH_4H_2PO_4(s) \rightarrow Sr_2P_2O_7(s) + 3H_2O(g) + 2NH_3(g),$$

respectively.

After the synthesis, set 1 and set 2 were obtained by doping $Sr_2P_2O_7$ into ZrP_2O_7 and doping ZrP_2O_7 into $Sr_2P_2O_7$, respectively. Their crystal systems and changes in unit cell parameters were studied by X-ray powder diffraction. The knowledge about their bonding was obtained by infrared and Raman spectroscopic measurements. Moreover, SEM micrographs and EDX analysis revealed the surface morphologies and compositions of the samples. The presence of thermoluminescence properties samples were explored by taking the glow curves.

According to these data, we have concluded for the set 1 that the unit cell parameters of the other samples were gradually decreased from 8.248(6) to 8.233(8) Å since orthorhombic $Sr_2P_2O_7$ was doped into cubic ZrP_2O_7 and the IR and Raman work show that the vibrational bands of $P_2O_7^{4-}$ ion were observed in all samples. SEM images of set 1 demonstrate that particle sizes of the samples are around 1 μm. In EDX analysis of these samples, Sr peak was clearly observed for the samples D32–D38. None of the members of set 1 showed the availability of thermoluminescence property.

For the set 2, orthorhombic $Sr_2P_2O_7$ were obtained by solid state reaction with a = 8.900(2), b = 13.151(2), and c = 5.402(2) Å unit cell parameters. The unit cell parameters of the other samples (D39–D45) were

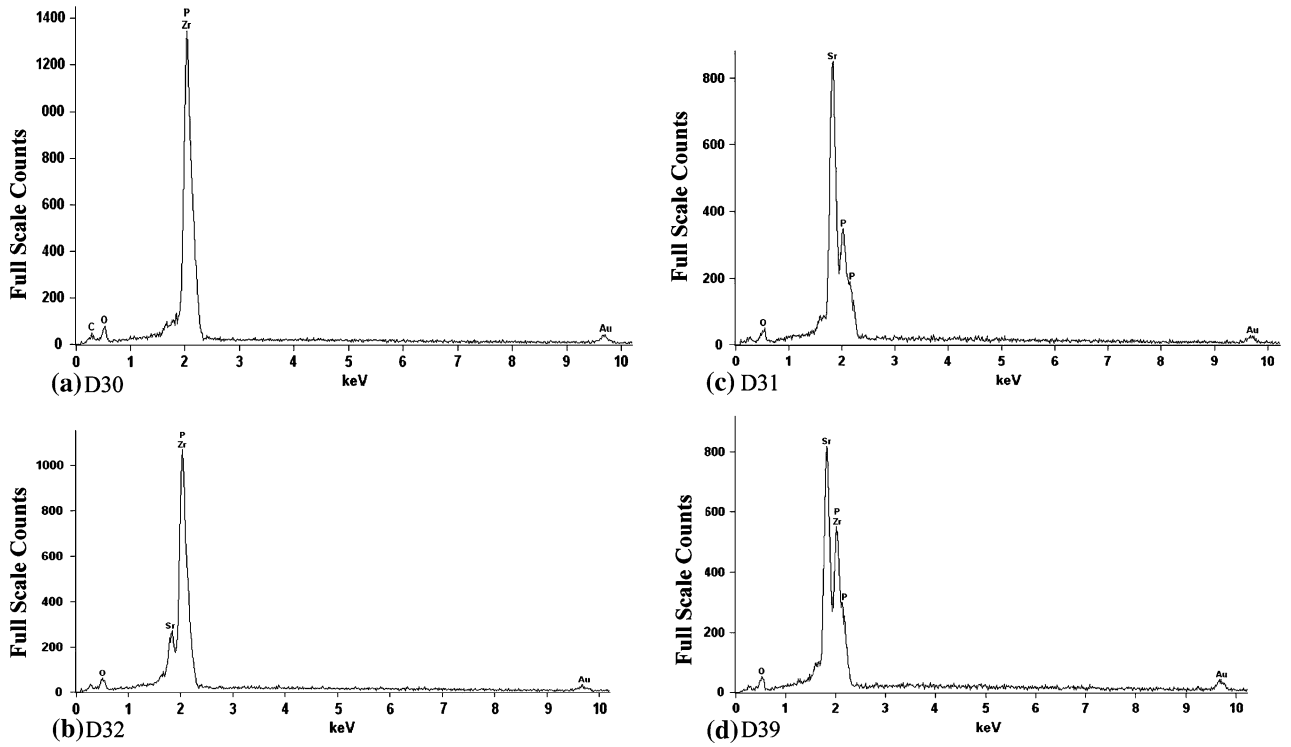

Fig. 10 EDX Analysis of D30, D32 from set 1, and D31, and D39 from set 2

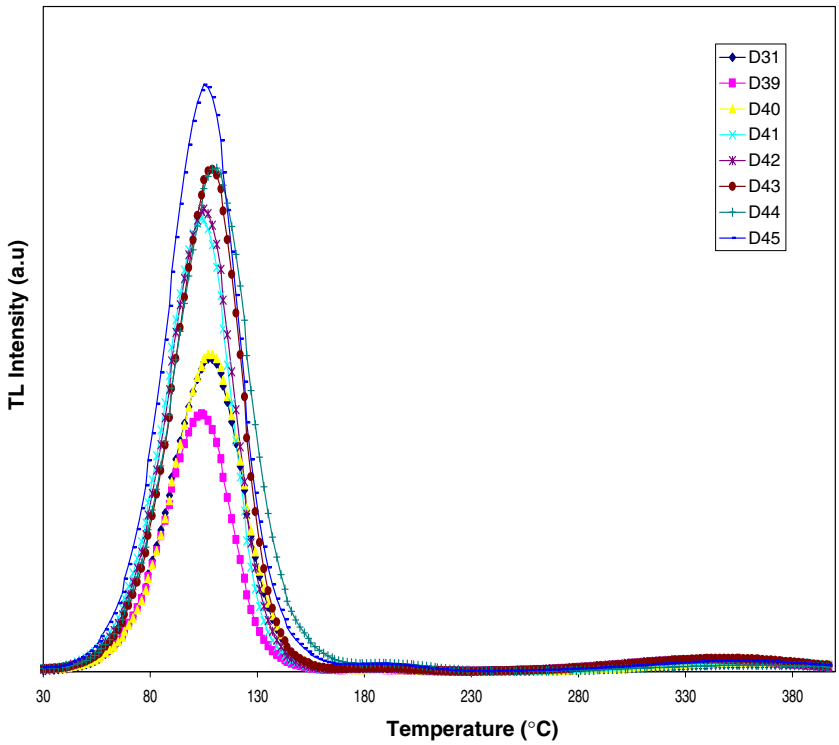

Fig. 11 Thermoluminescence glow curves of set 2

fluctuate in between a = 8.909(5)–8.877(5), b = 13.163(3)–13.12(1), and c = 5.403(2)–5.386(4) Å. The cubic ZrP_2O_7 (a = 24.74(1) Å) molecule is the reason for these changes. The vibrational data demonstrate that some coincidences in IR and Raman were observed. The inserted SEM images show larger

particles for the samples in set 2 and in the compositional analysis; Zr peak was found in all of the doped samples.

The glow curves of the set 2 exhibit one strong glow peak at around 100 °C. The intensity of prominent glow peak at 100 °C is continuously increased with decreasing concentration of ZrP_2O_7 among the set 2. The TL sensitivity of these samples when compared with the well known dosimetric material LiF:Mg,Ti (TLD-100), it was observed that their sensitivities are much more than TLD-100. This means that the responsible defect with main peak increases with decreasing concentration of ZrP_2O_7.

With these findings, we can conclude that unit cell parameters of the both sets did not much altered from doping and structures of cubic ZrP_2O_7 and $Sr_2P_2O_7$ were stable during doping while making solid solutions, and the ZrP_2O_7 doped $Sr_2P_2O_7$ type solid solutions are potential thermoluminescent materials.

Acknowledgement This work was supported by BAP-01-03-DPT-03K-120920/09. The authors also dedicated this paper to the memory of Meral Kızılyallı.

References

1. Withers RL, Tabira Y, Evans JSO, King IJ, Sleight AW (2001) J Solid State Chem 157:186
2. Khosrovani N, Korthuis V, Sleight AW (1996) Inorg Chem 35:485
3. Lisnyak VV, Stus NV, Slobodyanik NS, Belyavina NM, Markiv VYA (2000) J Alloys Compd 309:83
4. Gover RKB, Withers ND, Allen S, Withers RL, Evans JSO (2002) J Solid State Chem 166:42
5. Chernaya VV, Mitaev AS, Chizhov PS, Dikarev EV, Shapanchenko RV, Antipov EV, Korolenko MV, Fabritchnyi PB (2005) Chem Mater 17:284
6. Guler H, Kurtulus F (2005) J Mater Sci 40:6565
7. Smaalen SV, Dinnebier R, Hanson J, Gollwitzer J, Bullesfeld F, Prokofiev A, Assmus W (2005) J Solid State Chem 178:2225
8. Kizilyalli M, Darras M (1993) J Solid State Chem 107:373
9. Kizilyalli M (1987) J Less-Common Metals 127:147
10. Tie SL, Li YY, Yang YS (1997) J Phys Chem Solids 58(6):957
11. Ferid M, Horchani-Naifer K (2004) Mater Res Bull 39:2209
12. Ferid M, Horchani K, Amami J (2004) Mater Res Bull 39:1949
13. Hamady A, Zid MF, Jouini T (1994) J Solid State Chem 113:120
14. Trunov VK, Oboznenko YV, Sirotikin SP, Tskhelashvili NB (1990) Inorg Mater 27(9):1993
15. Trunov VK, Oboznenko YV, Sirotikin SP, Tskhelashvili NB (1991) Inorg Mater 27(11):2370–2374
16. Ledain S, Leclaire A, Borel MM, Raveau B (1996) Acta Cryst C42:1593
17. Boutfessi A, Boukhari A, Holt EM (1996) Acta Cryst C42:1594
18. Boutfessi A, Boukhari A, Holt EM (1996) Acta Cryst C42:1597
19. Khay N, Ennaciri AA, Harcharras M (2001) Vib Spectrosc 27:119
20. Khay N, Ennaciri AA (2001) J Alloys Compd 323–324:800
21. Idrissi MS, Rghioui L, Nejjar R, Benarafa L, Idrissi MS, Lorriaux A, Wallart F (2004) Spectrochim Acta Part A 60:2043
22. Stock N, Ferey G, Cheetham AK (2000) Solid State Sci 2:307
23. Assaaoudi H, Butler IS, Kozinski J, Belanger-Gariepy F (2005) J Chem Crystallogr 35(10):809
24. Varga T, Wilinson AP, Haluska MS, Payzant EA (2005) J Solid State Chem 178:3541
25. Pelova VA, Grigorov LS (1997) J Luminescence 72–74:241
26. Kim CH, Yim HS (1999) Solid State Commun 110:137
27. Marcu IC, Millet JMM, Herrmann JM (2002) Catal Lett 78(1–4):273
28. Inoue S, Ohtaki N (1993) J Chromatogr 645(1):57
29. Srilakshmi Ch, Ramesh K, Nagaraju P, Lingaiah N, Prasad PSS (2006) Catal Lett 106(3–4):115
30. Fukuda K, Moriyama A, Hashimoto S (2004) J Solid State Chem 177:3514
31. Natarajan V, Bhide MK, Dhobale AR, Godbole SV, Seshagari TK, Page AG, Lu CH (2004) Mater Res Bull 39:2065
32. Altermatt UD, Brown ID (1987) Acta Cryst A34:125
33. Pillai VPM, Thomas BR, Nayar VU, Lii KH (1999) Spectrochim Acta Part A 55:1809
34. Baran EJ, Mercader RC, Massafero A, Kremer E (2004) Spectrochim Acta Part A 60:1001